RSC Advances

PAPER

View Article Online
View Journal | View Issue

Cite this: *RSC Adv.*, 2026, **16**, 17983

Molecular blueprints for cleaner air: theoretical insights into Cu(I)-decorated heterocycles for greenhouse gas ($CO/CO_2/CH_4$) capture

Abhishek Bag [ab] and Gourisankar Roymahapatra *[b]

This study presents a comprehensive DFT investigation on Cu(I)-decorated five-membered aromatic heterocycles—imidazole, pyrazole, thiazole, oxazole, isoxazole, and isothiazole—as molecular hosts for capturing key greenhouse gases (CO, CO_2, and CH_4). Geometry optimization and electronic-structure analyses (B3LYP/6-31+G(d,p)) were combined with adsorption-energy evaluation, CDFT descriptors, NBO charge distribution, NICS, PDOS, ELF, NCI analyses, ADMP dynamics, and Gibbs free-energy profiling to establish structure–property relationships governing gas uptake. Most Cu-heterocycle hosts accommodate up to four gas molecules, with adsorption strength following the consistent trend CO > CO_2 > CH_4. CO adsorption is strongly chemisorptive, supported by significant charge transfer and Cu → CO π-back donation, whereas CO_2 and CH_4 show progressively weaker interactions. Aromaticity is largely preserved after adsorption, and ADMP simulations confirm good kinetic stability of all hosts. Thermodynamic analysis reveals spontaneous CO binding, moderately favourable CO_2 capture, and marginal CH_4 adsorption at room temperature. Gravimetric storage capacities reach ~39–46% (CO), ~54–57% (CO_2), and ~30–33% (CH_4). Among all systems, Cu(I)-decorated imidazole and oxazole frameworks emerge as the most efficient and stable hosts. These insights provide clear electronic and structural design rules for developing next-generation Cu-based adsorbents tailored for selective and high-capacity greenhouse-gas capture.

Received 6th November 2025
Accepted 10th March 2026

DOI: 10.1039/d5ra08553e

rsc.li/rsc-advances

1. Introduction

Since the emergence of metal–organic frameworks (MOFs) in the mid-1990s, researchers have been actively investigating porous materials to enable more efficient gas storage and separation.[1–4,2,3,] Early studies demonstrated that frameworks containing open metal sites or functional organic linkers could strongly interact with small molecules such as CO, CO_2, and CH_4, laying the foundation for advanced gas-capture technologies.[5–8] Today, MOFs and related porous materials are considered promising candidates for removing greenhouse gases (GHGs) from industrial exhaust streams and environmental sources.[9,10]

Greenhouse gases—including CO_2, CH_4, CO, and fluorinated gases—are major contributors to global warming and atmospheric deterioration, arising mainly from fossil-fuel combustion, industrial activities, deforestation, agriculture, and waste management.[11–13] Their accumulation in the atmosphere elevates global temperatures and causes harmful environmental and health impacts. To mitigate these effects, significant effort has been directed toward developing materials that can selectively capture, store, or convert GHGs before they are released into the environment. Materials such as MOFs, COFs, zeolites, activated carbon, and clay-based adsorbents have shown considerable promise due to their tunable pore environments and chemical versatility.[14–17]

Computational chemistry has become a powerful tool in accelerating such material discoveries. Density functional theory (DFT) and molecular-dynamics simulations enable scientists to examine gas–adsorbent interactions at the atomic level, screen promising structures, and predict performance before experimental synthesis.[16,17] These approaches significantly reduce cost, time, and material waste, thereby supporting the rapid exploration of new adsorbent architectures.

At present, gas-capture technologies are applied primarily in large-scale industrial settings such as coal-fired power plants, chemical factories, and refineries. Innovations in direct air capture, CO_2-to-fuel conversion, and renewable-energy integration indicate a strong global shift toward sustainable carbon-management solutions.[18–22] However, challenges such as high operating costs, energy requirements, and limited long-term stability still restrict widespread implementation.

Over the last decade, both synthetic and theoretical studies have reported numerous high-performance frameworks capable of storing H_2, CH_4, and CO_2 efficiently.[23–27] MOFs—constructed from metal ions such as Zr, Cu, Zn, Al, Fe, and Mg—remain the

[a]*Dept. of Basic Science and Humanities, Global Institute of Science and Technology, ICARE Complex, Haldia 721657, WB, India*

[b]*School of Applied Sciences and Humanities, Haldia Institute of Technology, ICARE Complex, Haldia 721657, WB, India. E-mail: grm.chem@gmail.com; grm.chem@hithaldia.in*

most widely studied due to their high porosity, structural stability, and tunable adsorption sites.[28–31] COFs, being lightweight and composed of light elements (C, H, B, N), also offer excellent potential for gas storage and separation.[27] Large-scale computational screening has further supported the identification of next-generation adsorbents and structure–property trends.[31]

In this context, metal-decorated heterocyclic molecules have emerged as promising building blocks for gas capture, owing to their strong coordination ability, electronic tunability, and chemical stability. Particularly, five-membered aromatic heterocycles offer well-defined binding pockets for metal ions and maintain aromatic rigidity, making them ideal candidates for selective gas adsorption.

The present study aims to explore Cu(I)-decorated five-membered aromatic heterocycles (imidazole, pyrazole, thiazole, oxazole, isoxazole, and isothiazole) as efficient molecular hosts for trapping CO, CO_2, and CH_4. Using DFT-based computational tools, we systematically analyze their adsorption capability, stability, electronic behavior, and thermodynamic feasibility. The goal is to establish clear structure–property relationships that can guide the rational design of future Cu-based gas-capture materials with high selectivity and storage performance.

2. Methodology and computational details

The designed systems are optimized to its local minimum on the potential energy surface with zero imaginary frequency with the help of the Gaussian 16w quantum chemistry program package[32] within density functional theory (DFT)[33] framework. Conceptual Density Functional Theory (DFT), as developed by Parr, Pearson, Chattaraj and co-workers, provides a set of global reactivity descriptors—such as chemical hardness (η), electrophilicity (ω)—that offer valuable insights into the electron-transfer behavior, intrinsic stability, and reactivity patterns of molecular systems. These descriptors are directly related to the frontier molecular orbitals and help rationalize how readily a system donates or accepts electron density during chemical interactions. In the context of gas adsorption, harder systems with larger HOMO–LUMO gaps tend to be more stable and less reactive, whereas species with higher electrophilicity exhibit an enhanced ability to accept electron density from incoming adsorbates such as CO or CO_2. To complement these global indices, we also employ the electron localization function (ELF) and non-covalent interaction (NCI) analysis, which provide spatial visualization of bonding, charge concentration, and weak intermolecular forces. Together, these conceptual and topological tools allow us to interpret not only the magnitude of adsorption energies but also the underlying nature of Cu–gas interactions, enabling a deeper understanding of the molecular factors that govern greenhouse-gas trapping efficiency. We have taken the functional B3LYP and basis sets like 6-31 + g(d,p). Basis set was used in their Cartesian form, and the optimizations were conducted in Cartesian coordinates without imposing symmetry constraints, allowing full relaxation of every structural parameter.

To ensure numerical stability and reproducibility, the self-consistent field (SCF) procedure used an energy convergence criterion of 10^{-8} a.u., along with density and orbital gradient thresholds of 10^{-6}. Geometry optimizations employed tight thresholds, with a maximum force of 1.5×10^{-5} a.u., RMS force of 1.0×10^{-5} a.u., maximum displacement of 6.0×10^{-5} a.u., and RMS displacement of 4.0×10^{-5} a.u. Schwarz integral screening for Coulomb integrals was applied with a cut off of 10^{-12}, and single-value decomposition (SVD) stabilization was activated automatically when required to address linear dependencies. No level-shifting was applied to the unoccupied orbitals during SCF unless convergence difficulties occurred; in such cases, a temporary shift of 0.5 a.u. was used and removed for final calculations.

The exchange–correlation potential was evaluated using the ultrafine integration grid (99 radial × 590 angular points) with Becke's partitioning scheme. Harmonic vibrational frequency calculations were performed at the same level of theory using analytic second derivatives to confirm that all optimized structures correspond to true minima (no imaginary frequencies). The computed vibrational data were used to obtain zero-point energies, enthalpy corrections, entropy contributions, and Gibbs free energies at 298 K and 250 K, following the standard rigid-rotor harmonic-oscillator (RRHO) formalism implemented in Gaussian. The stability and chemical reactivity of the Cu(I)-AH systems and their CO_2/CO/CH_4 (GHGs) adsorbed complexes have been analyzed by different conceptual DFT (CDFT) based descriptors like hardness (η) and electrophilicity (ω), calculated with standard techniques.[34–37] The average binding energy (E_b) value of each Cu(I)-AH systems are determined using eqn (1)

$$E_b = [E_{(rCu)^+@nGHGs} - (E_{(rCu)^+} + nE_{GHGs})]/n \quad (1)$$

where $E_{(rCu)^+@nGHGs}$, $E_{(rCu)^+}$ & E_{GHGs} represent the energy of the gradual GHGs adsorbed Cu(I)-AH system, only Cu(I)-AH system and energy of GHGs molecule. Here 'n' symbolizes the number of GHGs molecules adsorbed.

The calculation of average adsorption energy (E_{ads}) of GHGs molecules is done by using eqn (2),

$$E_{ads} = -E_b/n \quad (2)$$

We have Calculated the NICS (0) and NICS (1) (Nucleus Independent Chemical Shift) values to check the pattern of aromaticity and stability of the different Cu(I)-AH systems as well as for Cu(I)-AH–nGHGs systems.[38–41] It is now possible to have both the σ and π aromatic property by calculating the NICS(0) and NICS(1) values. The sign of NICS value determines the aromatic property. The negative and positive NICS value refers the aromatic and anti-aromatic nature, respectively. NICS (0) is typically computed at ring center, which provides the σ electron delocalization whereas NICS(1) *i.e.*, at point 1 Å above the ring center was recommended as being a better measure of the π electron delocalization. After development of NICS criteria, the term 'aromaticity' has been used for inorganic and metal–organic hybrid molecules. To calculate the Gas storage

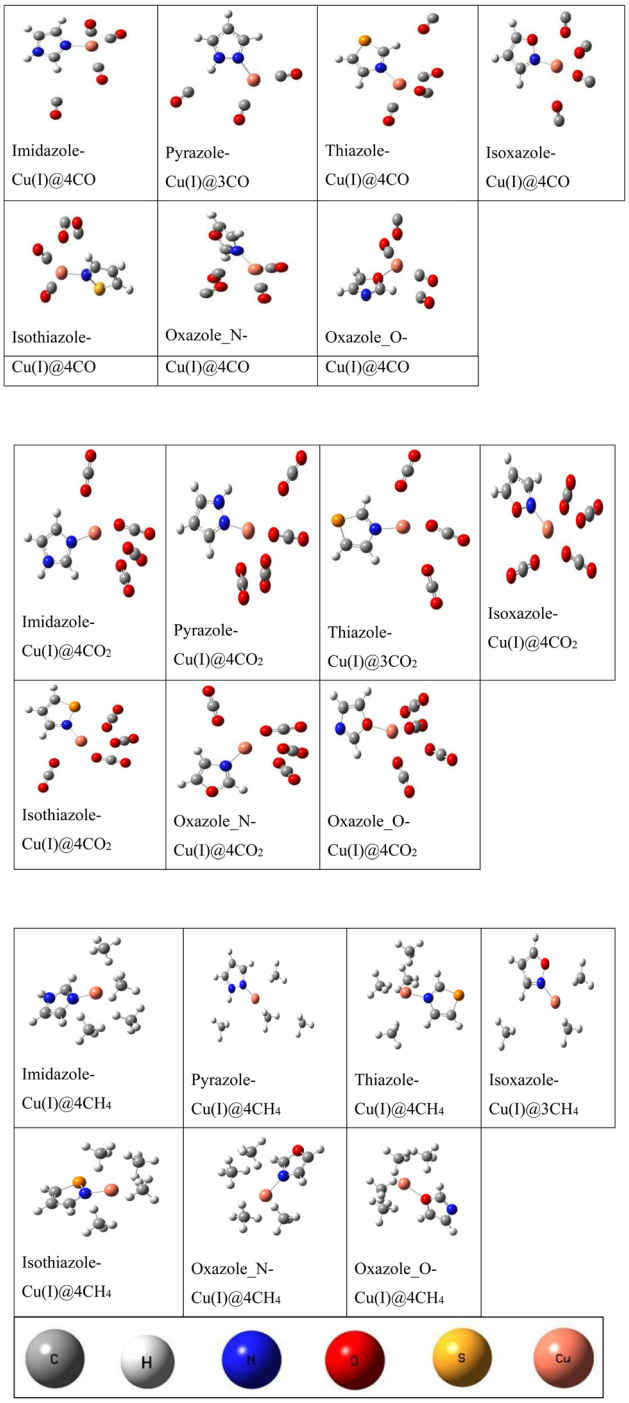

Fig. 1 Optimized structure of maximum GHGs adsorb different aromatic five-membered heterocyclic systems decorated with Cu(I) at B3LYP/6–31+g (d, p) level of theory.

efficiency of our studied systems we have calculated gravimetric wt% with the help of the eqn (3),

$$\text{Gravimetric wt\%} = \frac{\text{Molecular weight of trapped GHGs}}{\text{Molecular weight of (rCu)} + \text{@nGHGs}} \times 100 \quad (3)$$

We have also calculated Gibbs free energy change with variation of temperature to know about the spontaneous nature of the GHGs adsorption process by using the following eqn (4)

$$\Delta G_{(\mathrm{rCu})^{+}@n\mathrm{GHGs}} = [G_{(\mathrm{rCu@GHGs})^{+}} - G_{(\mathrm{rCu})^{+}} - nG_{n\mathrm{GHGs}}] \quad (4)$$

To know the bonding nature inside the different systems we have performed the topological analysis with the help of the

Table 1 Maximum number of GHGs that are adsorb by the different Cu(I) decorated model systems at B3LYP/6–31+g (d, p) level of theory

	No. of GHG molecules adsorb		
Systems	CO_2	CO	CH_4
Imidazole-Cu@nGHG	4	4	4
Pyrazole-Cu@nGHG	4	3	4
Thiazole-Cu@nGHG	3	4	4
Oxazole_N-Cu@nGHG	4	4	4
Oxazole_O-Cu@nGHG	4	4	4
Isoxazole-Cu@nGHG	4	4	3
Isothiazole-Cu@nGHG	4	4	4

Table 2 Different bond distances of highest number of GHGs adsorb different model systems at B3LYP/6–31+g (d, p) level of theory

	Bond distance [Å]		
Systems [CO_2 adsorb]	Ring-Cu	Cu-GHG	C–O [adsorb CO_2 molecule]
Imidazole-Cu@4CO_2	1.889	2.927	1.167
Pyrazole-Cu@4CO_2	1.893	2.842	1.167
Thiazole-Cu@3CO_2	1.898	2.701	1.167
Oxazole_N-Cu@4CO_2	1.899	2.818	1.167
Oxazole_O-Cu@4CO_2	2.069	2.659	1.167
Isoxazole-Cu@4CO_2	1.906	2.709	1.166
Isothiazole-Cu@4CO_2	1.895	2.758	1.168
	Bond distance[Å]		
Systems [CO adsorb]	Ring-Cu	Cu-GHG	C–O [adsorb CO molecule]
Imidazole-Cu@4CO	2.035	2.842	1.132
Pyrazole-Cu@3CO	1.962	2.877	1.132
Thiazole-Cu@4CO	1.992	2.881	1.132
Oxazole_N-Cu@4CO	1.989	3.000	1.132
Oxazole_O-Cu@4CO	2.103	2.863	1.130
Isoxazole-Cu@4CO	1.901	2.647	1.145
Isothiazole-Cu@4CO	1.984	2.972	1.132
	Bond distance[Å]		
Systems[CH_4 adsorb]	Ring-Cu	Cu-GHG	C–H [adsorb CH_4 molecule]
Imidazole-Cu@4CH_4	1.897	3.341	1.101
Pyrazole-Cu@4CH_4	1.899	3.970	1.101
Thiazole-Cu@4CH_4	1.912	3.227	1.101
Oxazole_N-Cu@4CH_4	1.910	3.553	1.101
Oxazole_O-Cu@4CH_4	2.053	2.937	1.099
Isoxazole-Cu@3CH_4	1.907	3.437	1.101
Isothiazole-Cu@4CH_4	1.906	3.256	1.101

Multiwfn package.[42] Further, we have also calculated the shaded surface map and electron localization function (ELF), which indicates the information about the localized electron. NCI (non-covalent interaction) analysis provides a link for the identification of bonding interaction in different Cu(I)-AH–nGHGs systems.[43] The NCI results are generated by using Multiwfn software package.[42,44] Atom centered density matrix propagation (ADMP)[45–47] study has been carried out to know about the kinetic stability of model systems. Partial Density of States (PDOS) can be generated for different parts of the GHGs-adsorb metal-decorated complexes to identify the contribution of adsorb GHGs, decorated metal, and aromatic heterocyclic ring to the frontier molecular orbitals of the complexes.[48]

3. Result and discussion

The optimized molecular structures of maximum GHGs trapping condition [Fig. 1] shows how different aromatic five-membered heterocyclic systems—like imidazole, pyrazole, thiazole, oxazole (N and O variants), isoxazole, and isothiazole—decorated with Cu(I) ions, interact with major greenhouse gases (CO, CO_2, and CH_4). These Cu-decorated systems act as potential adsorbents, effectively trapping up to four molecules of these gases. Most systems capture 4 molecules of each gas [Table 1], indicating strong and consistent interaction. A few exceptions were noted: thiazole-Cu binds only 3 CO_2 molecules, isoxazole-Cu binds only 3 CH_4 molecules, and pyrazole-Cu binds only 3 CO molecules. This suggests that the nature of the heteroatom in the ring (like N, O, or S) and its position influences gas binding efficiency. Overall, these structures demonstrate the potential of Cu-decorated heterocycles for greenhouse gas trapping, which could be useful in designing materials for environmental gas capture and storage. All other lower number of GHGs trapping optimized structure is in Fig. SF1.

A comparative evaluation of the optimized bond distances [Table 2] reveals clear structural signatures associated with the trapping efficiency of the Cu(I)-decorated heterocycles toward CO_2, CO, and CH_4. For CO_2 adsorption, the Ring–Cu distances remain tightly clustered around 1.88–1.91 Å, except in Oxazole_O-Cu where a slightly elongated distance (2.069 Å) reflects the stronger electron-donating ability of the O-site. The Cu–CO_2 distances follow a similar consistency (2.65–2.92 Å), indicating stable physisorption-driven coordination across all systems, while the C–O bond of CO_2 remains practically unchanged ($\approx$1.167 Å), confirming the non-destructive nature of adsorption. In the case of CO trapping, the Ring–Cu distances show moderate expansion (1.90–2.10 Å), consistent with the stronger back-bonding interaction between Cu(I) and CO. The Cu–CO distances vary between 2.64–3.00 Å, with isoxazole exhibiting the shortest Cu–CO bond (2.647 Å), suggesting favorable orbital overlap, whereas oxazole_O displays the longest due to its electronic environment. The C–O bond remains largely preserved (1.130–1.145 Å), consistent with chemisorption that does not induce severe CO activation. For CH_4 capture, the Ring–Cu distances remain in the narrow 1.89–

Table 3 Electrophilicity (ω); (eV) and, hardness (η); (eV) of maximum number of GHGs adsorbed different model systems at B3LYP/6−31 + g (d, p) level of theory

Systems	Green house gas[GHG]					
	CO_2		CO		CH_4	
CDFT based descriptors	Hardness (η; eV)	Electrophilicity (ω; eV)	Hardness (η; eV)	Electrophilicity (ω; eV)	Hardness (η; eV)	Electrophilicity (ω; eV)
Imidazole-Cu@nGHG	6.128	4.771	4.684	7.489	6.443	4.576
Pyrazole-Cu@nGHG	6.198	4.993	4.487	9.179	6.464	4.919
Thiazole-Cu@nGHG	5.879	5.815	4.713	8.508	5.888	5.968
Oxazole_N-Cu@nGHG	6.249	5.147	4.826	8.557	6.475	5.319
Oxazole_O-Cu@nGHG	5.609	5.864	4.113	10.162	5.787	5.910
Isoxazole-Cu@nGHG	5.584	5.997	5.800	6.495	6.165	6.104
Isothiazole-Cu@nGHG	5.446	6.299	4.950	8.290	5.781	6.422

Table 4 NICS(0) and NICS(1); (ppm) values of different model systems at B3LYP/6−31+g (d, p) level of theory

System adsorb with CO	NICS(0) (ppm)	NICS(I) (ppm)	System adsorb with CO_2	NICS(0) (ppm)	NICS(I) (ppm)	System adsorb with CH_4	NICS(0) (ppm)	NICS(I) (ppm)
Imidazole-Cu@4CO	−12.791	−11.304	Imidazole-Cu@4CO_2	−12.974	−11.14	Imidazole-Cu@4CH_4	−12.945	−11.492
Pyrazole-Cu@3CO	−13.0226	−12.1017	Pyrazole-Cu@4CO_2	−2.796	−9.162	Pyrazole-Cu@4CH_4	−13.104	−11.908
Thiazole-Cu@4CO	−11.69	−11.731	Thiazole-Cu@3CO_2	−12.008	−12.898	Thiazole-Cu@4CH_4	−12.018	−11.888
Oxazole-N-Cu@4CO	−11.555	−10.414	Oxazole-N_Cu@4CO_2	−11.811	−10.401	Oxazole-N-Cu@4CH_4	−11.903	−10.427
Oxazole-O-Cu@4CO	−16.77	−9.527	Oxazole-O-Cu@4CO_2	−11.008	−20.619	Oxazole-O-Cu@4CH_4	−11.015	−25.388
Isoxazole-Cu@4CO	−11.321	−13.07	Isoxazole-Cu@4CO_2	−11.563	−13.446	Isoxazole-Cu@3CH_4	−11.622	−11.217
Isothiazole-Cu@4CO	−11.832	−12.366	Isothiazole-Cu@4CO_2	−12.017	−11.585	Isothiazole-Cu@4CH_4	−11.97	−11.806

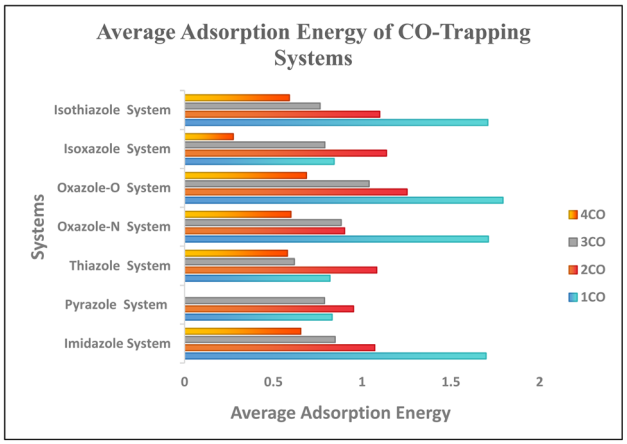

[A]

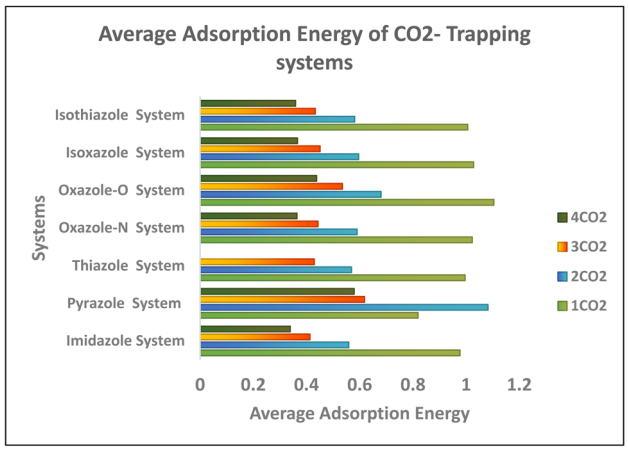

[B]

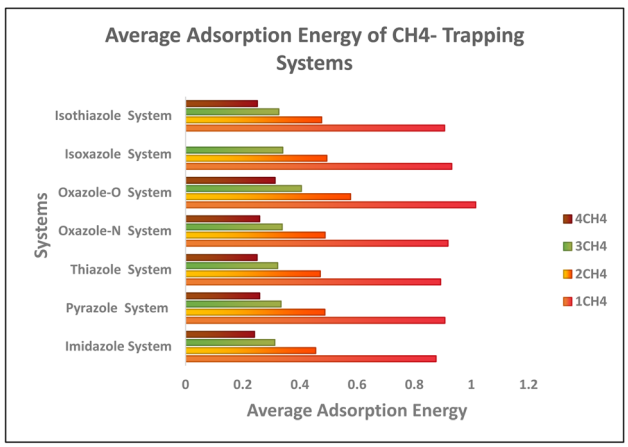

[C]

Fig. 2 Variation of E_{ads} (eV) (average adsorption energy) with the gradual adsorption of different GHGs molecules ([A] for CO, [B] for CO_2 and [C] for CH_4) for different model systems decorated with Cu(I) at B3LYP/6–31+g (d, p) level of theory.The horizontal axis representing adsorption energy.

1.91 Å range for most systems, except for oxazole_O-Cu which again shows a slight elongation (2.053 Å). As expected for a weakly interacting molecule, Cu–CH_4 distances are the longest among all gases (3.22–3.97 Å), demonstrating dominant van der Waals interactions. The C–H distances (≈1.10 Å) remain essentially unchanged, further confirming minimal perturbation of the methane framework. Overall, these structural parameters collectively illustrate that CO establishes the strongest interaction with the Cu center, CO_2 exhibits moderate but uniform binding, and CH_4 shows the weakest interaction, fully consistent with the observed adsorption energy trends and the selective gas-trapping capability of the Cu(I)-heterocycle hosts.[49,50]

The interaction of greenhouse gases (GHGs) such as CO_2, CO, and CH_4 with various Cu-decorated heterocyclic frameworks demonstrates intriguing electronic properties and gas-trapping capacities, as reflected in their conceptual density functional theory (CDFT) descriptors (Table 3). Among the studied systems—imidazole, pyrazole, thiazole, oxazole (N- and O-coordinated), isoxazole, and isothiazole-based Cu frameworks, all display the capability to trap up to four molecules of each gas, with minor variations. Oxazole_O-Cu@nGHG stands out by exhibiting the highest electrophilicity (ω = 10.162) for CO, indicating a strong tendency to accept electrons, which enhances CO adsorption. Isoxazole-Cu@nGHG shows remarkable CH_4 electrophilicity (ω = 6.104), suggesting its effectiveness in methane capture. Furthermore, isothiazole-Cu@nGHG presents a balanced profile, combining high electrophilicity with consistently good trapping numbers across all gases, highlighting its potential as a versatile gas sorbent. Interestingly, the highest hardness values for CO_2 are found in oxazole_N-Cu@nGHG (η = 6.249), indicating greater stability and less polarizability, which may enhance selectivity. The overall data suggest that a synergistic interplay between electronic hardness and electrophilicity governs the adsorption behavior. Systems with moderately high hardness and elevated electrophilicity, such as oxazole_O and isothiazole variants, may offer optimal performance by balancing stability and reactivity. These findings emphasize the potential of fine-tuning electronic properties through heterocyclic backbone engineering and Cu-functionalization to design next-generation materials for greenhouse gas mitigation. The graphical representations and values of Electrophilicity and hardness of lower number of GHGs trapping systems are in Fig. SF2 and Table ST1.

The Nuclear Independent Chemical Shift (NICS) values provide a reliable measure of aromaticity, where more negative values indicate stronger aromatic character. The Table 4 data for Cu(I)-decorated aromatic heterocycles adsorbed with maximum number of different greenhouse gases (CO, CO_2, and CH_4) shows that most systems retain significant aromaticity after gas adsorption, as reflected by their highly negative NICS(0) and NICS(1) values. Among them, oxazole-O-Cu exhibits the most pronounced aromaticity, especially when adsorbed with CH_4, showing extremely negative NICS(1) values, suggesting enhanced ring current effects. Imidazole-Cu and pyrazole-Cu also maintain strong aromaticity across all gases, although pyrazole-Cu shows a marked reduction in NICS(0) with CO_2, indicating some disturbance in the π-electron delocalization. In contrast, systems like isoxazole-Cu and isothiazole-Cu display consistent aromatic stability with minimal variation between gases, implying that their aromatic

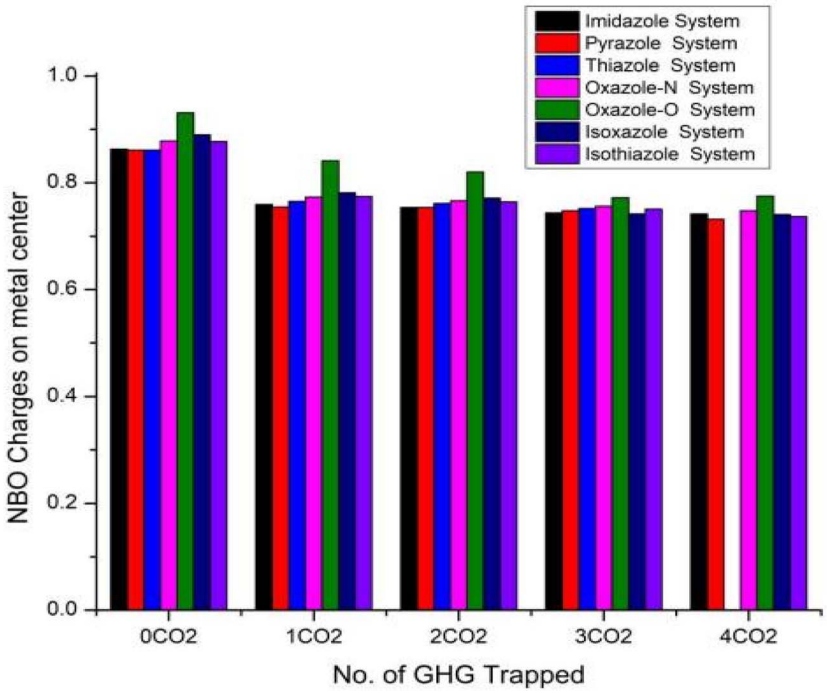

Fig. 3 Variation of NBO charges on Cu center in hosts and their sequential different GHGs adsorb systems (for CO_2.).

frameworks are less perturbed by adsorption. Overall, the results reveal that Cu(I) decoration supports the preservation of aromatic character in these heterocycles, with certain systems showing even stronger aromaticity upon specific gas trapping, which could be advantageous for selective greenhouse gas capture applications.

The adsorption energy data from Fig. 2 shows how effectively Cu-decorated aromatic heterocyclic rings can adsorb different GHGs (CO, CO_2, and CH_4). For CO, the highest adsorption is generally observed when only one molecule is adsorbed, with Oxazole-O (1.793 eV) and Imidazole (1.698 eV) performing notably well, indicating strong binding in these systems. As more CO molecules are introduced, the adsorption energy decreases steadily across all systems, reflecting saturation of active sites. For CO_2, the trend is similar—single-molecule adsorption shows stronger interaction, with Oxazole-O again leading (1.104 eV), while multiple CO_2 molecules result in lower energies. Methane (CH_4) shows comparatively weaker adsorption overall, but Oxazole-O maintains the highest performance (1.015 eV for a single molecule). Across all gases, Oxazole-O and Imidazole consistently show higher adsorption energies, suggesting they have more favorable active sites for gas capture. The general decline in energy with increasing gas numbers highlights the limited capacity and competitive occupation of adsorption sites. These patterns indicate that while Cu-decoration enhances gas binding, especially for CO and CO_2, the efficiency strongly depends on the heterocycle type and the number of molecules adsorbed.[51,52] To demonstrate the adsorption strength of the Cu(I)-decorated aromatic heterocycles, we compared the calculated CO, CO_2, and CH_4 adsorption energies with reported values for other single-atom or metal-doped systems. In our study, the first CO adsorption on Cu(I)-decorated heterocycles lies in the range 1.60–1.79 eV, with Oxazole-O-Cu(I) showing the highest value (1.793 eV). These values are significantly higher than many previously reported single-atom adsorbents.

For example, CO adsorption on Ag-ZSM-5 is 1.323 eV,[53] on Si-doped graphene only 0.190 eV,[54] and on Y-doped Ti_2CO_2 0.917 eV.[55] Thus, the Cu(I)-heterocycles reported here exhibit stronger CO binding than these benchmark systems, highlighting their superior interaction strength and potential for selective CO capture. Similarly, CO_2 and CH_4 adsorption energies in our systems also fall within or above typical ranges reported for single-atom decorated nanostructures, further supporting their applicability as efficient GHG-trapping hosts.

This comparison clearly strengthens the significance of our results and demonstrates that Cu(I)-decorated heterocycles provide a highly active adsorption platform, competitive with or better than many known single-atom adsorbents. The Average Adsorption values of metal decorated model systems at gradual GHGs adsorbing condition are in Table ST2.

The NBO charge analysis of the Cu center (Fig. 3) clearly shows how electron density rearranges when CO_2 gas interact with the Cu-decorated heterocycles. In the unbound state, the Cu atoms carry relatively high positive charges, with Oxazole-O displaying the highest value (0.931) and other systems such as Imidazole and Pyrazole showing slightly lower charges around 0.86. Upon CO adsorption, the positive charge on Cu decreases markedly, especially when several CO molecules are bound. This strong reduction reflects significant electron back-donation from CO to the metal center. For example, in the Imidazole system the Cu charge drops from 0.863 (no gas) to

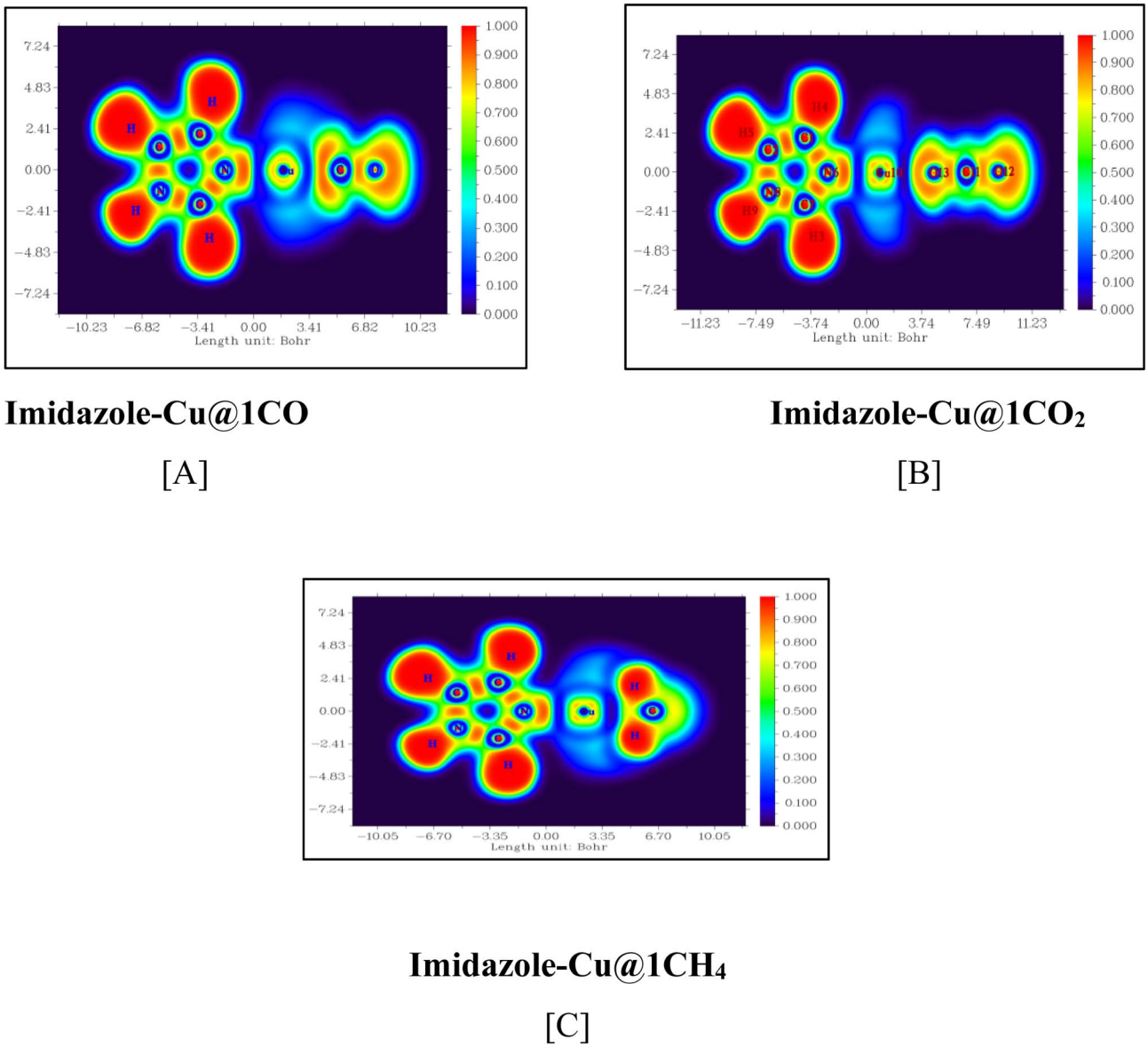

Fig. 4 ELF plot of different GHGs adsorb ([A] for CO, [B] for CO_2 and [C] for CH_4) imidazole systems decorated with Cu(I) at B3LYP/6–31+g (d, p) level of theory.

nearly neutral (−0.029) when three to four CO molecules are attached, demonstrating intense metal–gas interaction. CO_2 adsorption leads to a more moderate charge decrease, consistent with its weaker electron-donor ability and predominantly physisorptive binding. CH_4 produces only minor changes, which aligns with its non-polar character and very weak interaction with Cu. Across all systems, Oxazole-O generally keeps the Cu center more positively charged, indicating a comparatively electron-deficient and more electrophilic metal site. Overall, these trends show that CO interacts most strongly with Cu, followed by CO_2, while CH_4 exhibits the weakest effect—highlighting clear gas-selectivity patterns and the electronic influence of different heterocyclic ligands.[56,57] The corresponding NBO charge values and the graph of CO and CH_4 adsorption for all systems are summarized in Fig. SF3 and Table ST3.

Fig. 4 presents the ELF analysis for the imidazole-based Cu(I) system, which shows the most representative behavior among the studied hosts. The ELF maps clearly illustrate how the Cu center interacts with different greenhouse gases and how the nature of these interactions varies with each molecule. The strong Cu–N bond in the imidazole ring provides a stable anchoring site for adsorption. For CO, the ELF distribution reveals pronounced electron sharing between the gas molecule and the Cu center, reflecting strong π-back-donation and making CO the most strongly bound species. CO_2 shows a weaker interaction, mainly through one of its oxygen atoms, consistent with its limited electron-donor ability. In contrast, CH_4 exhibits only very weak, diffuse interactions with the Cu center because it lacks lone pairs and significant polarity.[58] These observations reinforce the adsorption trend CO > CO_2 >

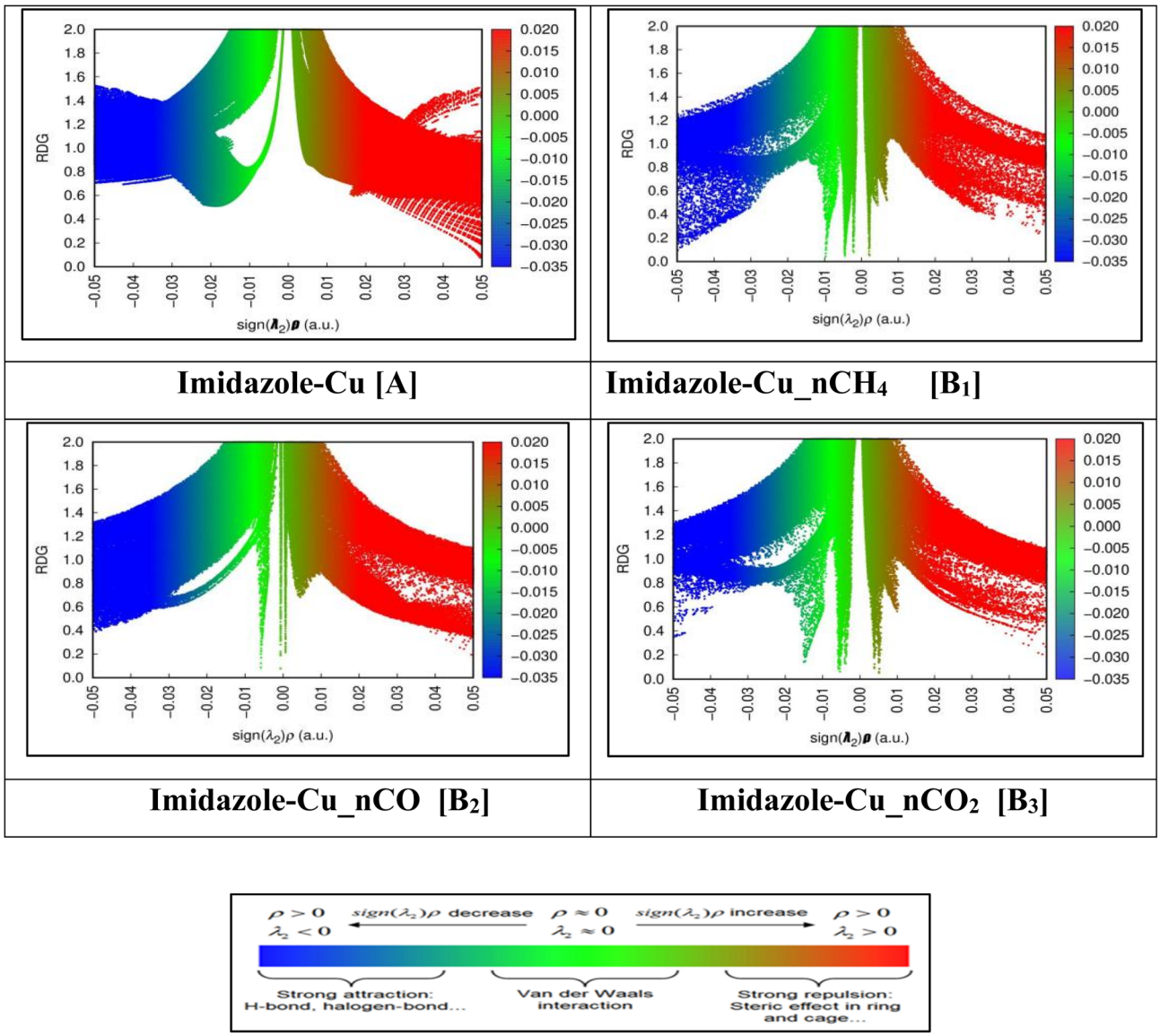

Fig. 5 NCI plot of different GHGs adsorb imidazole systems decorated with Cu(I) at B3LYP/6–31+g (d, p) level of theory without [A] and with [B]([B_1] for CH_4, [B_2] for CO and [B_3] for CO_2) trapping condition.

CH_4, demonstrating that the electronic nature of each gas governs its trapping capability. ELF plots for the remaining systems are provided in Fig. SF4.

The non-covalent interaction (NCI) study(Fig. 5) helps us understand how greenhouse gases like CH_4, CO, and CO_2 interact with copper(I)-decorated imidazole systems.[59] [As Imidazole systems show the better results]. This interaction is not a strong chemical bond but a weak force that holds gas molecules gently on the surface without damaging the system. First, the copper ion forms a stable bond with the nitrogen atom in the imidazole ring, creating a site that can attract and adsorb gas molecules. When methane (CH_4) interacts with this system,

Table 5 Gibbs free energy change [eV] at different temperature of different GHGs adsorb model systems decorated with Cu(I) at B3LYP/6–31 + g (d, p) level of theory

GHGs	Imidazole system		Pyrazole system	Thiazole system		Oxazole-N system	Oxazole-O system	Isoxazole system		Isothiazole system
Temp	298 K	250 K	298 K	298 K	250 K	298 K	298 K	298 K	250 K	298 K
CO	−0.925	—	−1.117	−0.874	—	−0.911	−1.219	0.131	−1.306	−0.885
CO_2	−0.108	—	−0.197	−0.296	—	−0.201	−0.449	−0.251	—	−0.179
CH_4	0.022	−0.466	−0.083	0.047	−0.477	−0.057	−0.166	−0.213	—	−0.001

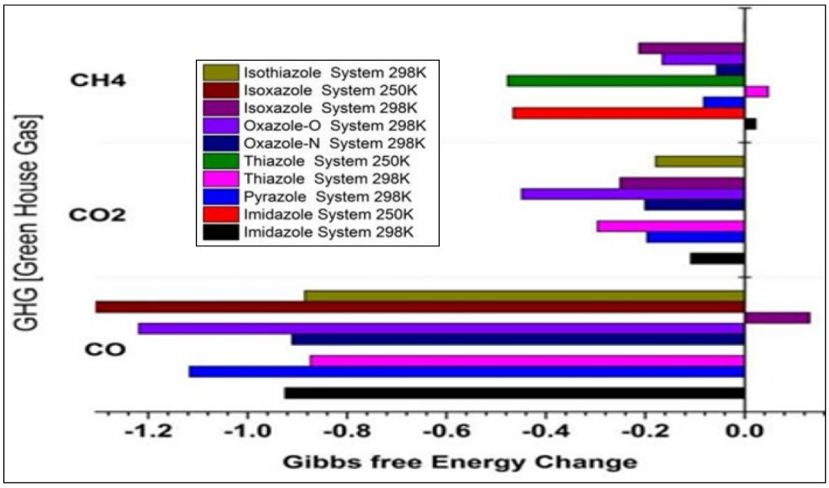

Fig. 6 Gibbs free energy change at different temperature of highest GHGs adsorb model systems decorated with Cu(I) at B3LYP/6–31+g (d, p) level of theory.

the bonding is very weak and happens through van der Waals forces. These are simple, physical attractions, and the NCI plots show green areas indicating such weak interactions. Since CH_4 has no dipole or lone pairs, it cannot form strong bonds, so it stays loosely attached. In the case of carbon monoxide (CO), the interaction is slightly stronger. CO has a lone pair of electrons on the oxygen atom, which can weakly interact with the copper ion. This creates small blue patches in the NCI plot, showing a weak attractive interaction. Still, the main bonding is van der Waals type, just a bit stronger than CH_4. Carbon dioxide (CO_2) shows the best interaction among the three gases. It has two oxygen atoms, which can both interact weakly with copper or hydrogen atoms on the imidazole ring. The NCI plots show more green areas and sometimes faint blue areas, indicating weak but meaningful bonding. Across all systems, no red areas were observed in the plots, meaning there is no repulsion or structural strain. Overall, the Cu–imidazole system remains stable while trapping gases through weak, reversible interactions. CO_2 binds the strongest, followed by CO, and CH_4 the weakest. This makes the system useful for gas sensing or reusable gas capture applications.

The Gibbs free energy analysis (Table 5) provides clear insight into the thermodynamic favorability of greenhouse-gas adsorption on the Cu(I)-decorated heterocycles. At room temperature (298 K), CO adsorption remains highly favorable across all systems, showing consistently negative ΔG values that reflect strong metal–gas interactions. CO_2 adsorption is moderately favorable, with ΔG values becoming less negative at higher temperatures, indicating a gradual weakening of its binding strength. In contrast, CH_4 exhibits the least favorable thermodynamics, with small or slightly positive ΔG values, consistent with its weak, nonpolar interaction with the Cu center. Overall, the ΔG trends reinforce the selectivity order CO > CO_2 > CH_4, in full agreement with the adsorption energies and electronic analyses reported in this study.

The graphical representation of Gibbs free energy change values [Fig. 6] indicates at room temperature or near room temperature, the gas adsorption process is spontaneous.[60,61]

Fig. 7 presents the Partial Density of States (PDOS) and the corresponding HOMO (highest occupied molecular orbital) and LUMO (lowest unoccupied molecular orbital) structures of Cu-decorated imidazole and pyrazole systems, each interacting with different greenhouse gases—CO_2, CO, and CH_4. PDOS analysis provides insight into how electronic states are distributed near the Fermi level and helps us understand how Cu and the heterocyclic ligands interact with the gases. In the Cu(I) decorated Imidazole [Imidazole system shows the best results] when exposed to CO_2 and CO, noticeable changes in the PDOS suggest strong interactions between the Cu center and the gas molecules. These shifts are less pronounced in the case of CH_4, indicating weaker interactions due to methane's non-polar nature. The HOMO structures in the CO_2 and CO systems are typically more localized near the Cu site and the gas molecule, pointing to charge transfer or orbital overlap. In contrast, CH_4 systems show less orbital involvement, highlighting a more physisorptive interaction. The LUMO levels also shift depending on the adsorbed gas, reflecting changes in the electron affinity and potential for reactivity. For example, in CO_2 and CO systems, lower LUMO energy levels suggest better electron-accepting capabilities, which could facilitate further chemical reactivity or electron transfer processes. Overall, the PDOS combined with the HOMO–LUMO distribution reveals how Cu-functionalized heterocycles exhibit selective sensitivity toward different greenhouse gases, especially CO_2 and CO. This understanding is useful for designing materials for gas sensing or captures applications. The visualization of electronic changes upon gas trapping helps in identifying the nature and strength of interaction—whether physisorption or chemisorption—thereby contributing to material optimization strategies.[62]

ADMP is like a super-zoomed, slow-motion video that watches both electrons and atoms move when a gas sticks to

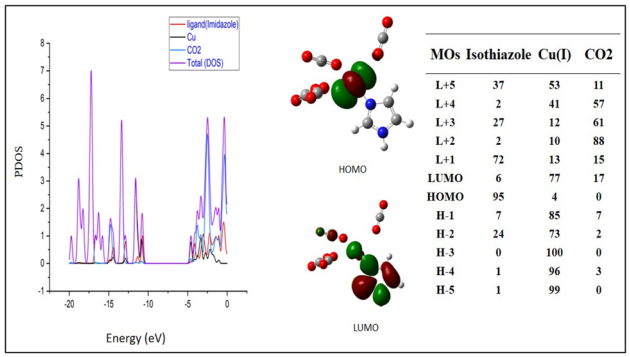

MOs	Isothiazole	Cu(I)	CO2
L+5	37	53	11
L+4	2	41	57
L+3	27	12	61
L+2	2	10	88
L+1	72	13	15
LUMO	6	77	17
HOMO	95	4	0
H-1	7	85	7
H-2	24	73	2
H-3	0	100	0
H-4	1	96	3
H-5	1	99	0

Imidazole Cu@nCO$_2$ systems

[A]

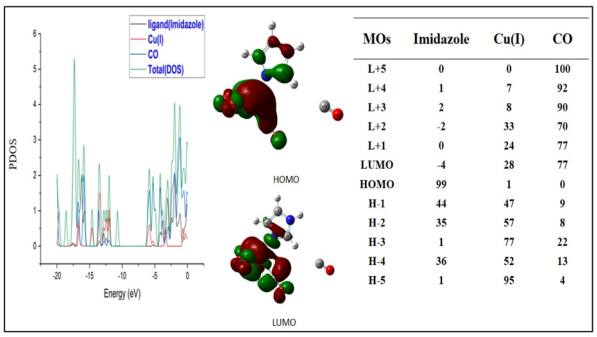

MOs	Imidazole	Cu(I)	CO
L+5	0	0	100
L+4	1	7	92
L+3	2	8	90
L+2	-2	33	70
L+1	0	24	77
LUMO	-4	28	77
HOMO	99	1	0
H-1	44	47	9
H-2	35	57	8
H-3	1	77	22
H-4	36	52	13
H-5	1	95	4

Imidazole Cu@nCO systems

[B]

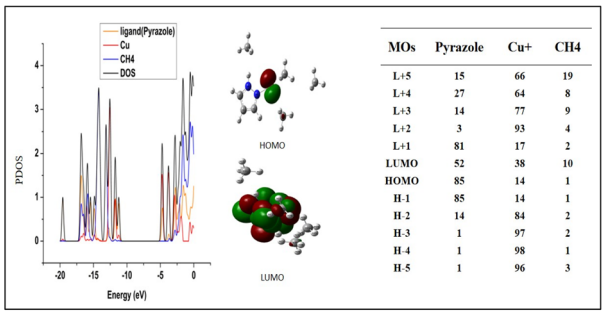

MOs	Pyrazole	Cu+	CH4
L+5	15	66	19
L+4	27	64	8
L+3	14	77	9
L+2	3	93	4
L+1	81	17	2
LUMO	52	38	10
HOMO	85	14	1
H-1	85	14	1
H-2	14	84	2
H-3	1	97	2
H-4	1	98	1
H-5	1	96	3

Imidazole Cu@nCH$_4$ systems

[C]

Fig. 7 DOS, PDOS and % of contribution of ring, metal ion and adsorb GHGs towards FMOs and HOMO–LUMO picture of different GHGs adsorb ([A] for CO_2, [B] for CO and [C] for CH_4) model systems decorated with Cu(I) at B3LYP/6–31+g (d, p) level of theory.

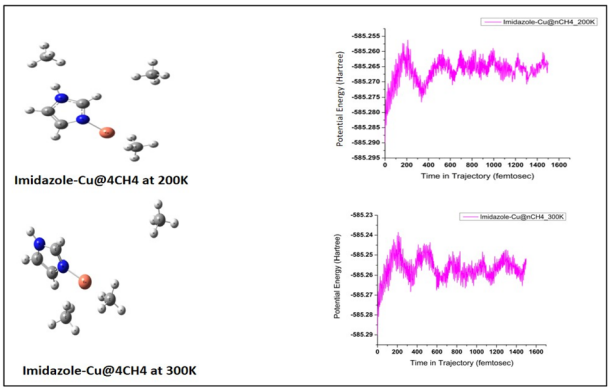

[A]

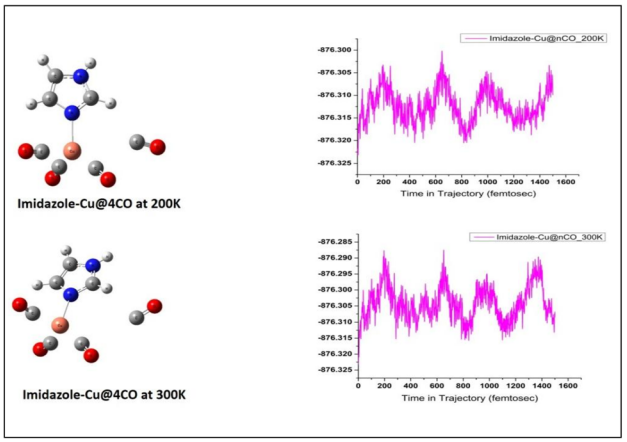

[B]

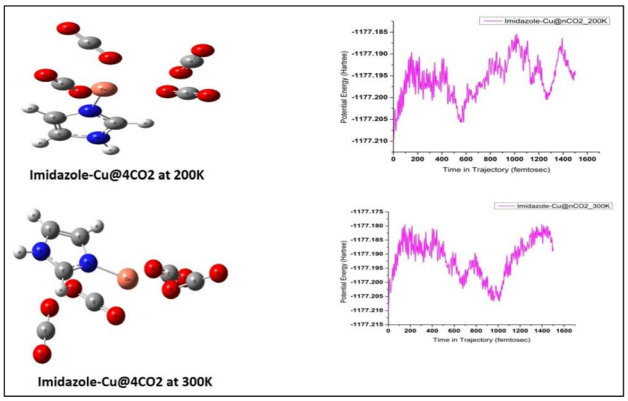

[C]

Fig. 8 The simulated structures and the potential energy (E, a.u.) *versus* time (t, fs) of different model systems decorated with Cu(I) [A(CH_4),B(CO) and C(CO_2)] at B3LYP/6–31+g (d, p) level of theory at 200 K and 300 K, as well as at 1500 fs.

copper on an imidazole ring. In Fig. 8, carbon monoxide holds on the strongest—its pull shows up as big, slow-fading waves in the electron cloud and small shifts in the copper's position. Carbon dioxide makes medium-sized ripples that disappear more quickly, and methane barely moves anything—just tiny, fast-fading wiggles. When we cool the system from 300 K to 200 K, everything slows down: even small disturbances last longer and look clearer. Because the size and lifetime of these waves match how tightly each gas binds, ADMP gives us a simple, dynamic "fingerprint" for CO, CO_2, and CH_4 all in one go. This helps chemists see exactly which gases stick best to copper-imidazole materials and how to make them even better at trapping greenhouse gases.[55]

Table 6 indicates the gravimetric weight percentage (Grv. wt%) values highlight the gas storage potential of Cu(I)-decorated aromatic heterocycles when trapping different greenhouse gases. Across all systems, from Fig. 9, CO_2 storage shows the highest gravimetric capacity, often exceeding 54–57%, which aligns with recent research trends where CO_2 capture is prioritized due to its significant role in climate change. CO storage also exhibits substantial values, ranging from about 39% to 46%, reflecting strong interaction and

Table 6 Gravimetric wt% values of maximum number of GHGs adsorb different model systems decorated with Cu(I) at B3LYP/6−31+g (d, p) level of theory

System	Grv. wt%	System	Grv. wt%	System	Grv. wt%
Imidazole-Cu@4CO	46.117	Imidazole-Cu@4CO_2	57.342	Imidazole-Cu@4CH_4	32.887
Pyrazole-Cu@3CO	39.092	Pyrazole-Cu@4CO_2	57.342	Pyrazole-Cu@4CH_4	32.887
Thiazole-Cu@4CO	43.107	Thiazole-Cu@3CO_2	47.16	Thiazole-Cu@4CH_4	30.237
Oxazole-N-Cu@4CO	45.931	Oxazole-N-Cu@4CO_2	57.172	Oxazole-N-Cu@4CH_4	32.701
Oxazole-O-Cu@4CO	45.931	Oxazole-O-Cu@4CO_2	57.172	Oxazole-O-Cu@4CH_4	32.701
Isoxazole-Cu@4CO	45.931	Isooxazole-Cu@4CO_2	57.172	Isooxazole-Cu@4CH_4	32.721
Isothiazole-Cu@4CO	43.107	Isothiazole-Cu@4CO_2	54.339	Isothiazole-Cu@4CH_4	30.237

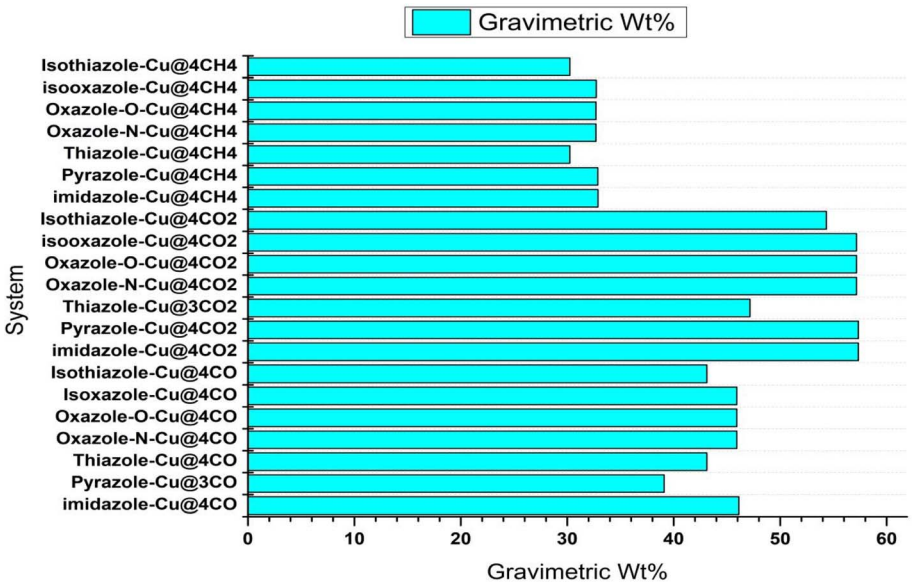

Fig. 9 Graphical representation of gravimetric wt% values of maximum number of green house gases adsorb different model systems decorated with Cu(I) at B3LYP/6−31+g (d, p) level of theory.

efficient packing within the frameworks. In contrast, CH_4 storage capacities are comparatively lower, typically between 30–33%, consistent with the lighter molecular weight and weaker binding affinity of methane. Among the studied systems, imidazole-Cu and pyrazole-Cu show notably high capacities for CO_2, while thiazole- and isothiazole-based models present balanced performance across gases. These results indicate that Cu(I) decoration not only preserves the structural integrity of these heterocycles but also optimizes their sorption efficiency, especially for CO_2, making them promising candidates in the modern pursuit of high-capacity, selective gas storage materials.[63,64]

Although the primary calculations in this study were performed at the B3LYP/6-31+G(d,p) level, we conducted an additional validation using the dispersion-inclusive long-range corrected ωB97X-D functional for the representative Imidazole–Cu(I)–CO adsorption system. The comparison (Table 7) clearly shows that both the optimization energies and the adsorption energies (*E*_ads) obtained with B3LYP closely agree with those computed using ωB97X-D. The variation in adsorption energy between the two functionals remains small (typically 0.03–0.06 eV), and the predicted decreasing trend in adsorption strength from 1CO → 4CO is perfectly preserved across both methods. This strong consistency indicates that the qualitative and quantitative conclusions of this work—particularly the relative stability, adsorption behavior, and gas-binding trends—are not significantly affected by the lack of explicit dispersion correction in the primary B3LYP calculations. Moreover, the excellent agreement with the ωB97X-D results reinforces that the electron-donation/back-donation mechanism and the structural trends captured here remain valid and reliable. Therefore, the findings presented in this study are fully supported by

Table 7 Comparison of the optimization energies and CO average adsorption energies (*E*_ads) obtained using B3LYP/6-31+G(d,p) and the dispersion-corrected ωB97X-D/6-31+G(d,p) methods for the Imidazole–Cu(I)@nCO systems

	Optimization energy (eV)		Eads (eV)	
Systems	B3LYP	ωB97X-D	B3LYP	ωB97X-D
Imidazole-Cu@1CO	−53871.852	−53868.647	1.698	1.659
Imidazole-Cu@2CO	−56955.817	−56951.626	1.071	1.102
Imidazole-Cu@3CO	−60039.741	−60034.575	0.848	0.907
Imidazole-Cu@ 4CO	−63123.337	−63117.116	0.654	0.707

a dispersion-corrected functional, ensuring robustness and scientific credibility while confirming that the chosen B3LYP level provides an accurate description of the systems investigated.

4. Conclusion

This study demonstrates that Cu(I)-decorated five-membered aromatic heterocycles are effective molecular hosts for CO, CO_2, and CH_4 capture. DFT results show a consistent adsorption trend—CO > CO_2 > CH_4—driven by strong Cu–CO charge transfer, moderate CO_2 interaction, and weak CH_4 physisorption. Most systems can adsorb up to four gas molecules while maintaining structural and aromatic stability, supported by NBO, NICS, PDOS, ELF, NCI, and ADMP analyses. Thermodynamic data confirm spontaneous CO binding and moderately favorable CO_2 adsorption at room temperature. Gravimetric capacities reach ~54–57% for CO_2, ~39–46% for CO, and ~30–33% for CH_4, highlighting meaningful storage potential. Overall, Cu(I)-decorated imidazole and oxazole emerge as the most promising hosts. These findings offer clear design guidelines for developing next-generation Cu-based materials for selective and efficient greenhouse-gas capture.

Author contributions

AB: structure optimization, calculations, data curation, data validation and drafting the manuscript. GR: conceptualisation, data validation, data curation, overall project supervision, writing and editing the final manuscript.

Conflicts of interest

There are no conflicts to declare.

Data availability

Supplementary information (SI): detailed DFT results for Cu(I)-decorated five-membered heterocycles interacting with CO, CO_2, and CH_4. It includes optimized geometries, orbital energies, and gradual adsorption data up to four gas molecules. Additionally, electrophilicity, hardness, adsorption energies, and NBO charge analyses are systematically reported, along with graphical representations and ELF plots to illustrate electronic behavior and interaction trends. See DOI: https://doi.org/10.1039/d5ra08553e.

Acknowledgements

The author, G. Roymahapatra, sincerely acknowledges the research grant received from DST-SERB, Government of India, under the Teachers Associateship for Research Excellence (TARE) scheme (Grant No.: TAR/2022/000162). Both authors extend their heartfelt gratitude to the Royal Society of Chemistry (RSC), England, for considering our article under the full APC waiver scheme and for their encouragement and support. The authors also express their sincere thanks to Haldia Institute of Technology (HIT), Haldia, for providing the necessary infrastructure and facilities.

References

1 O. M. Yaghi, H. Li and T. L. Groy, Construction of porous solids from hydrogen-bonded metal complexes of 1,3,5-benzenetricarboxylic acid, *J. Am. Chem. Soc.*, 1996, **118**, 9096–9101, DOI: 10.1021/ja961601k.

2 J.-R. Li, R. J. Kuppler and H.-C. Zhou, Selective gas adsorption and separation in metal–organic frameworks, *Chem. Soc. Rev.*, 2009, **38**, 1477–1504, DOI: 10.1039/B802426J.

3 A. R. Millward and O. M. Yaghi, Metal–organic frameworks with exceptionally high capacity for storage of carbon dioxide at room temperature, *J. Am. Chem. Soc.*, 2005, **127**, 17998–17999, DOI: 10.1021/ja0570032.

4 J. Sculley, D. Yuan and H.-C. Zhou, The current status of hydrogen storage in metal–organic frameworks—updated, *Energy Environ. Sci.*, 2011, **4**, 2721–2735, DOI: 10.1039/C1EE01240A.

5 K. Sumida, D. L. Rogow, J. A. Mason, T. M. McDonald, E. D. Bloch, Z. R. Herm, T.-H. Bae and J. R. Long, Carbon dioxide capture in metal–organic frameworks, *Chem. Rev.*, 2012, **112**, 724–781, DOI: 10.1021/cr2003272.

6 T. M. McDonald, W. R. Lee, J. A. Mason, B. M. Wiers, C. S. Hong and J. R. Long, Capture of carbon dioxide from air and flue gas in the alkylamine-appended metal–organic framework mmen-Mg_2(dobpdc), *J. Am. Chem. Soc.*, 2012, **134**, 7056–7065, DOI: 10.1021/ja300034j.

7 W. L. Queen, M. R. Hudson, E. D. Bloch, J. A. Mason, M. I. Gonzalez, J. S. Lee, D. Gygi, J. D. Howe, K. Lee, T. A. Darwish, M. James, V. K. Peterson, S. J. Teat, B. Smit, J. B. Neaton, J. R. Long and C. M. Brown, Comprehensive study of carbon dioxide adsorption in the metal–organic frameworks M_2(dobdc) (M = Mg, Mn, Fe, Co, Ni, Cu, Zn), *Chem. Sci.*, 2014, **5**, 4569–4581, DOI: 10.1039/C4SC01932B.

8 T. G. Glover, G. W. Peterson, B. J. Schindler, D. Britt and O. M. Yaghi, MOF-74 building unit has a direct impact on toxic gas adsorption, *Chem. Eng. Sci.*, 2011, **66**, 163–170, DOI: 10.1016/j.ces.2010.06.007.

9 H.-C. Zhou, J. R. Long and O. M. Yaghi, Introduction to metal–organic frameworks, *Chem. Rev.*, 2012, **112**, 673–674, DOI: 10.1021/cr300014x.

10 Z. Chen, S. L. Hanna, L. R. Redfern, D. Alezi, T. Islamoglu and O. K. Farha, Reticular chemistry in the rational synthesis of functional zirconium cluster-based MOFs, *Coord. Chem. Rev.*, 2020, **423**, 213466, DOI: 10.1016/j.ccr.2020.213466.

11 IPCC, *Climate Change 2021: the Physical Science Basis. Contribution of Working Group I to the Sixth Assessment Report of the Intergovernmental Panel on Climate Change*, Cambridge University Press, 2021, https://www.ipcc.ch/report/ar6/wg1/.

12 U.S. Environmental Protection Agency (EPA), *Overview of Greenhouse Gases*, 2023, https://www.epa.gov/ghgemissions/overview-greenhouse-gases.

13 P. D. Wakchaure and B. Ganguly, Computational Study on Metal-Ion-Decorated Prismane Molecules for Selective Adsorption of CO_2 from Flue Gas Mixtures, *ACS Omega*, 2020, **5**, 31146–31155, DOI: 10.1021/acsomega.0c04299.

14 H. Furukawa, K. E. Cordova, M. O'Keeffe and O. M. Yaghi, The chemistry and applications of metal–organic frameworks, *Science*, 2013, **341**, 1230444, DOI: 10.1126/science.1230444.

15 R. Zhao, Y. Wang, X. Li, B. Sun and C. Wang, Porous materials for carbon dioxide capture: A review, *Environ. Chem. Lett.*, 2021, **19**, 1135–1164, DOI: 10.1007/s10311-020-01107-3.

16 Y. G. Chung, E. Haldoupis, B. J. Bucior, M. Haranczyk, S. Lee, H. Zhang, K. D. Vogiatzis, M. Milisavljevic, S. Ling, J. S. Camp, B. Slater, J. I. Siepmann, D. S. Sholl and R. Q. Snurr, Advances, updates, and analytics for the Computation-Ready, Experimental Metal–Organic Framework Database: CoRE MOF 2019, *J. Chem. Eng. Data*, 2019, **64**, 5985–5998, DOI: 10.1021/acs.jced.9b00835.

17 C. E. Wilmer, M. Leaf, C. Y. Lee, O. K. Farha, B. G. Hauser, J. T. Hupp and R. Q. Snurr, Large-scale screening of hypothetical metal–organic frameworks, *Nat. Chem.*, 2012, **4**, 83–89, DOI: 10.1038/nchem.1192.

18 International Energy Agency (IEA), Carbon Capture, Utilisation and Storage: Tracking Report, 2023, https://www.iea.org/reports/carbon-capture-utilisation-and-storage-2023.

19 J. Larsen, W. Herndon, S. Mohan and P. Marsters, *Net-Zero America: Carbon Capture and Storage*, Princeton University – Net-Zero America Project, 2021, https://netzeroamerica.princeton.edu.

20 V. S. Sikarwar, M. Reichert, M. Jeremias, V. Manovic, R. McKenna, P. S. Fennell and A. Valero, Progress in bio-based carbon capture technology, *J. Cleaner Prod.*, 2021, **278**, 123805, DOI: 10.1016/j.jclepro.2020.123805.

21 X. Li, J. Wang, C. Wang and Z. Zhang, Metal–organic frameworks for personal and portable environmental protection: Recent advances and future perspectives, *Adv. Funct. Mater.*, 2023, **33**, 2207895, DOI: 10.1002/adfm.202207895.

22 G. Centi and S. Perathoner, Opportunities and prospects in the chemical recycling of carbon dioxide to fuels, *Catal. Today*, 2009, **148**, 191–205, DOI: 10.1016/j.cattod.2009.07.075.

23 N. L. Rosi, J. Eckert, M. Eddaoudi, D. T. Vodak, J. Kim, M. O'Keeffe and O. M. Yaghi, Hydrogen storage in microporous metal–organic frameworks, *Science*, 2003, **300**, 1127–1129, DOI: 10.1126/science.1083440.

24 O. K. Farha, A. Ö. Yazaydin, I. Eryazici, C. D. Malliakas, B. G. Hauser, M. G. Kanatzidis, S. T. Nguyen, R. Q. Snurr and J. T. Hupp, De novo synthesis of a metal–organic framework material featuring ultrahigh surface area and gas storage capacities, *Nat. Chem.*, 2010, **2**, 944–948, DOI: 10.1038/nchem.834.

25 W. Zhou, H. Wu, M. R. Hartman and T. Yildirim, Hydrogen and methane adsorption in metal–organic frameworks: A high-pressure volumetric study, *Science*, 2012, **336**, 1018–1023, DOI: 10.1126/science.1217544.

26 F. Gándara and H. Furukawa, Chemistry of framework materials: Topology, stability, and functionalization of metal–organic frameworks, *Chem. Rev.*, 2014, **114**, 1057–1083, DOI: 10.1021/cr400605f.

27 A. P. Côté, A. I. Benin, N. W. Ockwig, M. O'Keeffe, A. J. Matzger and O. M. Yaghi, Porous, crystalline, covalent organic frameworks, *Science*, 2005, **310**, 1166–1170, DOI: 10.1126/science.1120411.

28 J. H. Cavka, S. Jakobsen, U. Olsbye, N. Guillou, C. Lamberti, S. Bordiga and K. P. Lillerud, A new zirconium inorganic building brick forming metal organic frameworks with exceptional stability, *J. Am. Chem. Soc.*, 2008, **130**, 13850–13851, DOI: 10.1021/ja8057953.

29 M. P. Suh, H. J. Park, T. K. Prasad and D. W. Lim, Hydrogen storage in metal–organic frameworks, *Chem. Rev.*, 2012, **112**, 782–835, DOI: 10.1021/cr200274s.

30 H. Li, M. Eddaoudi, M. O'Keeffe and O. M. Yaghi, Design and synthesis of an exceptionally stable and highly porous metal–organic framework, *Nature*, 1999, **402**, 276–279, DOI: 10.1038/46248.

31 C. E. Wilmer, M. Leaf, C. Y. Lee, O. K. Farha, B. G. Hauser, J. T. Hupp and R. Q. Snurr, Large-scale screening of hypothetical metal–organic frameworks, *Nat. Chem.*, 2012, **4**, 83–89, DOI: 10.1038/nchem.1192.

32 M. J. Frisch *et al.*, *Gaussian 16, Revision A.03*, Gaussian, Inc., Wallingford CT, 2016, https://gaussian.com.

33 R. G. Parr and W. Yang, *Density-functional Theory of Atoms and Molecules*, Oxford University Press, New York, 1989, DOI: 10.1007/978-94-009-9027-2_2.

34 R. G. Parr, Absolute hardness: companion parameter to absolute electronegativity, *J. Am. Chem. Soc.*, 1983, **105**, 7512, DOI: 10.1021/ja00364a005.

35 K. D. Sen and C. K. Jorgensen, *Electronegativity, Struct. Bonding*, Springer, Berlin, 1987, vol. 66, DOI: 10.1002/bbpc.19890930424.

36 R. G. Parr, L. V. Szentpaly and S. Liu, Electrophilicity Index, *J. Am. Chem. Soc.*, 1999, **121**, 1924, DOI: 10.1021/ja983494x.

37 P. K. Chattaraj, *Chemical Reactivity Theory: A Density Functional View*, CRC Press, Taylor and Francis, Boca Raton, FL, 2009, DOI: 10.1201/9781420065442.

38 Z. Chen, C. S. Wannere, C. Corminboeuf, R. Puchta and P. V. R. Schleyer, Nucleus-independent chemical shifts (NICS) as an aromaticity criterion, *Chem. Rev.*, 2005, **105**, 3842, DOI: 10.1021/cr030088+.

39 A. Bag, S. Sinha, H. S. Das, S. Giri, G. C. De, S. Maity, B. B. Xu, Z. Guo, J. Ganguly and G. Roymahapatra, Hydrogen Storage Efficiency of Ag(I)/Au(I) Decorated Five-Member Aromatic Heterocyclic (AH) Compounds: A Theoretical Investigation, *Eng. Sci.*, 2024, **28**, 1062, DOI: 10.30919/es1062.

40 A. Bag, S. Giri, P. Dhaiveegan, R. T. T. Jalgham, G. C. De, J. Ganguly and G. Roymahapatra, A Theoretical Study on Au(I) Decorated Isomeric Triazine Complexes as A New Class of Hydrogen Storage Materials, *ES Energy Environ.*, 2024, **23**, 1115, DOI: 10.30919/esee1115.

41 G. Roymahapatra, M. K. Dash, A. Ghosh, A. Bag, S. Mishra and S. Maity, Hydrogen Storage on Lithium Chloride/Lithium Bromide Surface at Cryogenic Temperature, *ES Energy Environ.*, 2022, **18**, 90–100, DOI: 10.30919/esee8c756.

42 T. Lu and F. W. Chen, Multiwfn: A multifunctional wavefunction analyzer, *J. Comput. Chem.*, 2012, **33**, 580, DOI: 10.1002/jcc.22885.

43 A. Ebrahimia, M. Izadyar and M. Khavanib, Theoretical design of a new hydrogen storage based on the decorated phosphorene nanosheet by alkali metals, *J. Phys. Chem. Solids*, 2023, **178**, 111354, DOI: 10.1016/j.jpcs.2023.111354.

44 H. O. Edeta, H. Louis, I. Benjamin, M. Gideon, T. O. Unimuke, S. A. Adalikwu, A. D. Nwagu and A. S. Adeyink, Hydrogen storage capacity of C12X12 (X = N, P, and Si), *Chem. Phys. Impact*, 2022, **5**, 100107, DOI: 10.1016/j.chphi.2022.100107.

45 R. F. W. Bader, P. J. MacDougall and C. D. H. Lau, Bonded and nonbonded charge concentrations and their relation to molecular geometry and reactivity, *J. Am. Chem. Soc.*, 2002, **106**, 1594–1605, DOI: 10.1021/JA00318A009.

46 H. B. Schlegel, J. M. Millam, S. S. Iyengar, G. A. Voth, A. D. Daniels, G. E. Scuseria, *et al.*, Ab initio molecular dynamics: Propagating the density matrix with Gaussian orbitals, *J. Chem. Phys.*, 2001, **114**, 9758, DOI: 10.1063/1.1372182.

47 S. S. Iyengar, H. B. Schlegel, J. M. Millam, G. A. Voth, G. E. Scuseria and M. J. Frisch, Ab initio molecular dynamics: Propagating the density matrix with Gaussian orbitals. II. Generalizations based on mass-weighting, idempotency, energy conservation and choice of initial conditions, *J. Chem. Phys.*, 2001, **115**, 10291, DOI: 10.1063/1.1416876.

48 G. Roymahapatra, M. K. Dash, S. Sinha, G. C. De and Z. Guo, Theoretical Investigation of Hydrogen Adsorption Efficiency of [Oxadiazole-xLi$^+$] Complexes (x = 1, 2); In Pursuit of Green Fuel Storage, *Eng. Sci.*, 2022, **19**, 114–124, DOI: 10.30919/es8d671.

49 A. Bag, M. K. Dash, E. Tarif, J. Z. Guo and G. Choudhury, Cu(I)-Decorated Five-Membered Aromatic Heterocyclic Complexes: A Potential Hydrogen Storage System, *ES Chem. Sustain.*, 2024, **1**, 221–230, https://www.espublisher.com/journals/articledetails/1311.

50 W. L. Queen, M. R. Hudson, E. D. Bloch, J. A. Mason, M. I. Gonzalez, J. S. Lee, D. Gygi, J. D. Howe, K. Lee, T. A. Darwish, M. James, V. K. Peterson, S. J. Teat, B. Smit, J. B. Neaton, J. R. Long and C. M. Brown, Comprehensive study of carbon dioxide adsorption in the metal–organic frameworks M_2(dobdc) (M = Mg, Mn, Fe, Co, Ni, Cu, Zn), *Chem. Sci.*, 2014, **5**, 4569–4581, https://tsapps.nist.gov/publication/get_pdf.cfm?pub_id=916344.

51 X. Li, Y. Zhao, H. Chen, J. Zhang, Y. Wang, W. Huang and J. Chen, N-Heterocyclic carbene-coordinated Cu single atoms on poly(ionic liquid) for efficient CO_2 electroreduction, *CCS Chem.*, 2025, **7**(4), 1495–1506, DOI: 10.31635/ccschem.024.202404829.

52 A. Bag, G. C. De, S. Bhattacharyya, B. Bepari, H. S. Das, S. Bandaru and G. Roymahapatra, Ag(I) Decorated Isomeric Triazine Complexes as Efficient Hydrogen Storage Materials – A Theoretical Investigation, *Chem. Inorg. Mater.*, 2025, **5**, 100093, DOI: 10.1016/j.cinorg.2025.100093.

53 Z.-Z. Qiu, Y.-X. Yu and J.-G. Mi, Adsorption of carbon monoxide on Ag(I)-ZSM-5 zeolite: An ab initio density functional theory study, *Appl. Surf. Sci.*, 2012, **258**(24), 9629–9635, DOI: 10.1016/j.apsusc.2012.05.162.

54 Yu Yang-Xin, Oxygen-transfer from N2O to CO via Y-doped Ti2CO2 (MXene) monolayer at room temperature: Density functional theory and ab initio molecular simulation studies, *J. Colloid Interface Sci.*, 2025, **695**, 137799, DOI: 10.1016/j.jcis.2025.137799.

55 R. Gholizadeh and Y.-X. Yu, N_2O + CO reaction over Si- and Se-doped graphenes: An ab initio DFT study, *Appl. Surf. Sci.*, 2015, **1**, 1187–1195, DOI: 10.1016/j.apsusc.2015.09.163.

56 X. Wang, C. Liu, F. Li, M. Liu and X. C. Zeng, DFT investigation of CO and NO adsorption on Cu_5Sc and Cu_6Sc^+ clusters: Insights from NBO charge analysis, *Comput. Theor. Chem.*, 2022, **1212**, 113694, DOI: 10.1016/j.comptc.2022.113694.

57 A. Bag, M. K. Dash, S. Giri, G. C. De and G. Roymahapatra, Hydrogen Storage Efficiency of Isomeric Cu(I)-Triazine Complexes: In Quest of New Hydrogen Storage Material, in *Computational Studies: from Molecules to Materials*, ed. A. K. Srivastava, CRC Press, Boca Raton, FL, USA, 2025, p. 228, DOI: 10.1201/9781003441328-12.

58 A. Bag, A. Aash, D. K. Debnath, G. N. Reddy and G. Roymahapatra, Exploring Reversible Hydrogen Storage Efficiency of R-Substituted [M-Doped Imidazoline-Li]$^+$ Complexes [R = $-CF_3$, –CN, $-CH_3$ and M = C, Si, Ge]; An In-Silico Study, *J. Eng. Ind. Res.*, 2025, **6**(3), 244–260, DOI: 10.48309/jeires.2025.514956.1185.

59 E. R. Johnson, S. Keinan, P. Mori-Sánchez, J. Contreras-García, A. J. Cohen and W. Yang, Revealing Noncovalent Interactions, *J. Am. Chem. Soc.*, 2010, **132**(18), 6498–6506, DOI: 10.1021/ja100936w.

60 Q. Yang and C. Zhong, Molecular simulation of carbon dioxide/methane/hydrogen mixture adsorption in metal–organic frameworks, *J. Phys. Chem. B*, 2006, **110**(36), 17776–17783, DOI: 10.1021/jp063821i.

61 Y. S. Bae and R. Q. Snurr, Development and evaluation of porous materials for carbon dioxide separation and capture, *Angew. Chem., Int. Ed.*, 2011, **50**(49), 11586–11596, DOI: 10.1002/anie.201101891.

62 B. Wang, A. P. Côté, H. Furukawa, M. O'Keeffe and O. M. Yaghi, Colossal cages in zeolitic imidazolate frameworks as selective carbon dioxide reservoirs, *Nature*, 2008, **453**, 207–211, DOI: 10.1038/nature06900.

63 P. D. Wakchaure and B. Ganguly, Computational Study on Metal-Ion-Decorated Prismane Molecules for Selective Adsorption of CO_2 from Flue Gas Mixtures, *ACS Omega*, 2020, **5**, 31146–31155, DOI: 10.1021/acsomega.0c04299.

64 X. Zhang, C. Liu, Y. Liu, R. Fan, F. Shi and X. Cui, Integrated CO_2 Capture and Conversion by a Robust Cu(I)-Based Metal–Organic Framework, *J. Am. Chem. Soc.*, 2024, **146**(39), 27006–27013, DOI: 10.1021/jacs.4c08757.